# States without a linear counterpart in Bose-Einstein condensates

Roberto D'Agosta[1,2,*] and Carlo Presilla[3,4,5,†]
[1]*Dipartimento di Fisica "E. Amaldi," Università di Roma Tre, via della Vasca Navale 84, Roma 00146, Italy*
[2]*Istituto Nazionale per la Fisica della Materia, Unità di Roma Tre, Roma 00146, Italy*
[3]*Dipartimento di Fisica, Università di Roma "La Sapienza," Piazzale A. Moro 2, Roma 00185, Italy*
[4]*Istituto Nazionale per la Fisica della Materia, Unità di Roma 1 and Center for Statistical Mechanics and Complexity, Roma 00185, Italy*
[5]*Istituto Nazionale di Fisica Nucleare, Sezione di Roma 1, Roma 00185, Italy*
(Received 23 March 2001; published 27 March 2002)

We show the existence of stationary solutions of a one-dimensional Gross-Pitaevskii equation in the presence of a multiwell external potential that do not reduce to any of the eigenfunctions of the associated Schrödinger problem. These solutions, which in the limit of strong nonlinearity have the form of chains of dark or bright solitons located near the extrema of the potential, represent macroscopically excited states of a Bose-Einstein condensate and are in principle experimentally observable.

DOI: 10.1103/PhysRevA.65.043609 PACS number(s): 03.75.Fi, 03.65.Ge, 42.65.Tg

## I. INTRODUCTION

Bose-Einstein condensation (BEC) of weakly interacting atomic gases [1] strongly motivates the study of the Gross-Pitaevskii equation (GPE),

$$\left[-i\hbar\frac{\partial}{\partial t}-\frac{\hbar^2}{2m}\nabla^2+U_0|\Psi(\boldsymbol{x},t)|^2+V(\boldsymbol{x})\right]\Psi(\boldsymbol{x},t)=0, \quad (1)$$

a mean-field Schrödinger equation with local cubic nonlinearity. Of particular interest are the nonground-state stationary solutions of the GPE [2,3] which represent macroscopically excited states of the condensate. Vortices have been recently observed in two- [4] or one-component [5] condensates and are also invoked as a superfluidity breaking mechanism [6]. Phase engineering optical techniques have allowed us to generate dark solitons in atomic gases with positive scattering length [7,8].

Vortices and solitons observed in recent experiments are examples of excited states with a linear counterpart, i.e., stationary solutions of the GPE which can be obtained as a deformation of eigenstates of the corresponding linear Schrödinger equation [9,10]. However, the GPE may also admit stationary solutions without a linear counterpart. In a discretized version of the GPE, also known as a discrete self-trapping equation, the existence and stability of solutions without a linear counterpart has been studied at various discretization orders [13]. In particular, the appearance of self-trapping stationary states in the dimer case, i.e., a two-level system approximating a double well, has been widely investigated in connection with the evolution of wave packets [14–16]. Recently, a set of stationary solutions without a linear counterpart has been discovered also in the continuous case, namely, the exactly solvable one-dimensional (1D) GPE with periodic boundary conditions and zero external potential [10]. These states break the rotational invariance of the associated linear problem.

In this paper, we show the existence of stationary solutions without a linear counterpart of a 1D GPE in the presence of a multiwell external potential. In the limit of strong nonlinearity, these solutions assume the form of chains of dark or bright solitons located near the extrema of the potential and in general break the symmetry of the external potential.

Our analysis is of direct interest for BEC experiments where atomic gases can be confined in almost arbitrarily tailored magnetic and optic traps [11,12]. As a case study, we investigate a GPE representing a quasi-1D Bose-Einstein condensate confined in a double-well trap described by the potential

$$V(x)=m^2\gamma^4x^4-m\omega^2x^2+\frac{\omega^4}{4\gamma^4}. \quad (2)$$

In Sec. III, we describe all the zero-, one-, and two-soliton solutions of this model in an analytical way valid in the limit of strong nonlinearity. In Sec. IV, by means of numerical simulations we find the exact shape of these states and study their evolution in the linear limit reached when the number of particles in the condensate $N$ vanishes. We consider both the cases of condensates with positive or negative scattering length. Shape and energy of the corresponding stationary solutions are shown in Figs. 1 and 3 and 2 and 4, respectively. Their stability properties are discussed in Sec. V.

## II. STATIONARY SOLUTIONS

Let us first review some general properties of the stationary solutions of the GPE that reduce, in the limit of vanishing nonlinearity, to the eigenfunctions of the associated Schrödinger equation

$$\left[-\frac{\hbar^2}{2m}\nabla^2+V(\boldsymbol{x})-\mathcal{E}_n\right]\phi_n(\boldsymbol{x})=0, \quad n=0,1,\ldots. \quad (3)$$

In [9] we have shown that for any finite value of the chemical potential $\mu$ there exists a set of stationary solutions of the GPE, $\Psi_{\mu n}(\boldsymbol{x},t)=\exp(-i/\hbar\mu t)\psi_{\mu n}(\boldsymbol{x})$, which have limit

*Electronic address: dagosta@fis.uniroma3.it
†Electronic address: carlo.presilla@roma1.infn.it

 

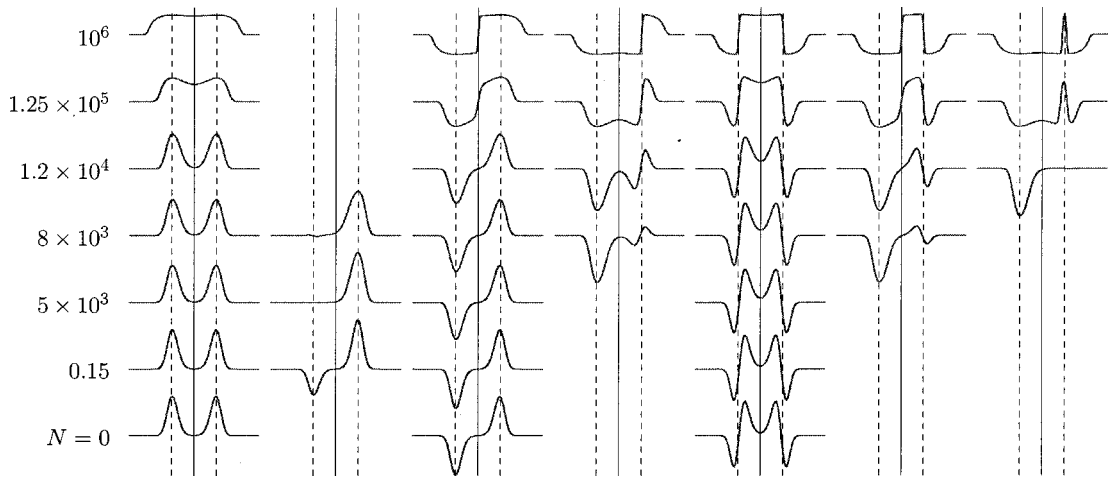


FIG. 1. Zero-, one-, and two-soliton stationary solutions of the repulsive GPE with the symmetric double-well potential (2) for different values of the normalization $N$. For comparison, the functions are shown scaled by $\sqrt{N}$. The vertical solid and dashed lines indicate the double-well maximum and minima, respectively. The degenerate states obtained by changing $\psi(x)\rightarrow\psi(-x)$ are not reported. The results have been obtained with the following parameters: $m=3.818\times10^{-26}$ kg, $\omega=12.75$ s$^{-1}$, $\gamma=10^9$ kg$^{-1/4}$ m$^{-1/2}$ s$^{-1/2}$, $U_0=1.1087\times10^{-41}$ J m, which correspond to sodium atoms confined in two quasiharmonic wells of angular frequency $\sim2\omega$ at distance $\sqrt{2\omega^2/m\gamma^4}\sim92$ $\mu$m.

$\psi_{\mu n}(\boldsymbol{x})\ \|\psi_{\mu n}\|^{-1}\rightarrow\phi_n(\boldsymbol{x})$ when $\mu\rightarrow\mathcal{E}_n$. The parameter $\mu$ ranges in the interval $[\mathcal{E}_n,+\infty)$ for $U_0>0$ and in the interval $(-\infty,\mathcal{E}_n]$ for $U_0<0$. In both cases, the number of particles in the state $\psi_{\mu n}$, $N_n(\mu)=\|\psi_{\mu n}\|^2$, vanishes for $\mu\rightarrow\mathcal{E}_n$. In other words, the linear limit is reached for a vanishing number of particles in the condensate.

In the 1D case, asymptotically exact expressions for the GPE stationary solutions with linear counterpart are known also in the opposite limit of strong nonlinearity. For $\mu\rightarrow\pm\infty$, depending on the sign of $U_0$, these solutions assume the form of chains of dark or bright solitons [9]. More specifically, in the repulsive case $U_0>0$ the solution with $n=0$ nodes assumes the zero-soliton shape

$$\psi_{\mu0}(x)\rightarrow\begin{cases}\sqrt{[\mu-V(x)]/U_0}, & \mu>V(x),\\ 0, & \mu<V(x),\end{cases}\tag{4}$$

while for $n\geqslant1$ nodes we obtain asymptotic solutions with $n$ dark solitons

$$\psi_{\mu n}(x)\rightarrow\psi_{\mu0}(x)\prod_{k=1}^{n}\tanh\left(\frac{\sqrt{m\mu}}{\hbar}(x-x_k)\right).\tag{5}$$

In the attractive case $U_0<0$, for $\mu\rightarrow-\infty$ the solutions with $n\geqslant0$ nodes give rise to $n+1$ bright solitons

$$\psi_{\mu n}(x)\rightarrow\sqrt{\frac{2\mu}{U_0}}\sum_{k=0}^{n}(-1)^k\,\mathrm{sech}\left(\frac{\sqrt{-2m\mu}}{\hbar}(x-x_k)\right).\tag{6}$$

In the functions (5) and (6) with two or more solitons, the solitons do not overlap, i.e., the distance between their centers $x_k$ is much larger than the dark-soliton width $\hbar/\sqrt{m\mu}$ or the bright-soliton width $\hbar/\sqrt{-2m\mu}$ [9]. Note that any sta-

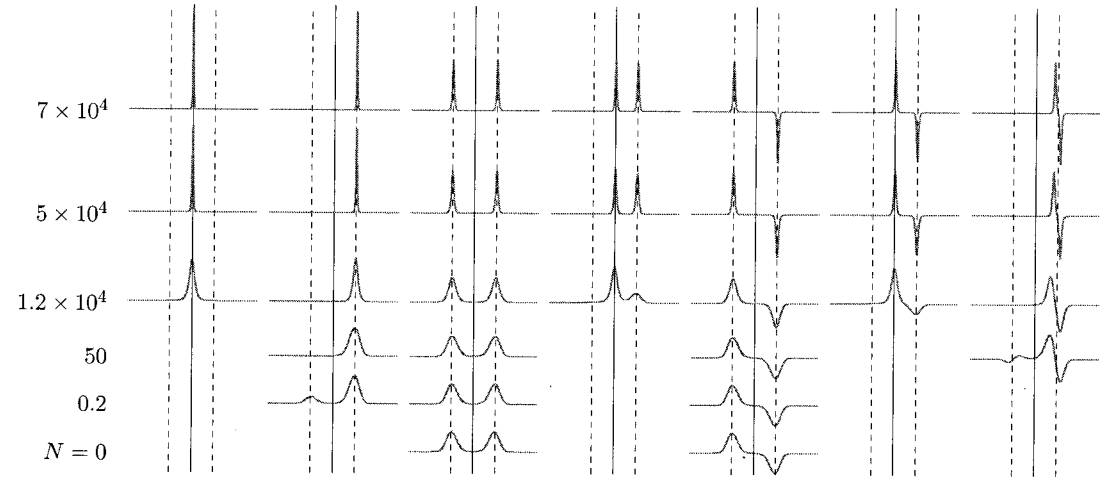


FIG. 2. As in Fig. 1 for the one- and two-soliton solutions in the attractive case $U_0=-1.1087\times10^{-41}$ J m.

tionary solution is invariant under a global phase change and we do not consider this trivial degeneracy.

The stationary solutions of the GPE, for $\mu$ fixed, are the critical points of the grand-potential functional

$$\Omega[\psi]=\int\left[\frac{\hbar^2}{2m}|\nabla\psi(\boldsymbol{x})|^2+\frac{U_0}{2}|\psi(\boldsymbol{x})|^4+[V(\boldsymbol{x})-\mu]\times|\psi(\boldsymbol{x})|^2\right]d\boldsymbol{x}. \tag{7}$$

Since for $|\mu|$ large the GPE solutions with a linear counterpart assume the forms (4)–(6) with some specified centers $\{x_k\}$, we look for more general multisoliton solutions in which the soliton centers may assume different values. The allowed $\{x_k\}$ can be determined by substituting the expressions (4)–(6) in Eq. (7) and extremizing the resulting function $\Omega(\{x_k\})$.

### III. ZERO-, ONE-, AND TWO-SOLITON SOLUTIONS IN A DOUBLE WELL

Zero-soliton solutions exist only in the repulsive case $U_0>0$ and are given by Eq. (4). For $\mu$ sufficiently large, we have a nodeless state which extends over the entire double well (column 1 of Fig. 1). If $\mu$ is smaller than the barrier height $\omega^4/4\gamma^4$, this state vanishes in the barrier region where $V(x)>\mu$. In this case, since $\psi=0$ is a trivial solution of the GPE, we could expect also two other stationary solutions of the form $\psi(x)=\sqrt{[\mu-V(x)]/U_0}$ in one of the two wells and $\psi(x)=0$ elsewhere [column 2 of Fig. 1 and symmetric partner $\psi(-x)$]. These latter solutions break the symmetry of $V$ and must disappear in the linear limit. They correspond to the self-trapped states studied in [13–16].

One-soliton solutions are described by Eq. (5) with $n=1$ in the repulsive case and Eq. (6) with $n=0$ in the attractive one. The corresponding grand potential becomes a function of the soliton centers $x_1$ or $x_0$, respectively. For $|\mu|$ sufficiently large, the width of the solitons is very small and the dependence of the integral (7) on $x_1$ or $x_0$ is due only to the term $V|\psi|^2$. The dark soliton density $|\psi_{\mu 1}|^2$ is constant with a hole in $x_1$ so that $\Omega(x_1)\sim$const.$-V(x_1)$. The bright soliton density $|\psi_{\mu 0}|^2$ is different from zero only in proximity of $x_0$ and $\Omega(x_0)\sim$const.$+V(x_0)$. In both cases we have three one-soliton solutions corresponding to the three extrema of the external potential. The soliton may be found in the maximum (column 3 of Fig. 1 and column 1 of Fig. 2) or in one of the two minima [column 4 of Fig. 1 and column 2 of Fig. 2 and symmetric partners $\psi(-x)$] of the double well. The two solutions with the soliton centers in $\pm x_m$, where $x_m=\sqrt{\omega^2/2m\gamma^4}$, break the symmetry of $V(x)$ and do not have a linear counterpart.

In the repulsive case, two-soliton solutions are described by Eq. (5) with $n=2$ and the grand potential becomes the two-variable function $\Omega(x_1,x_2)$. When the distance between the soliton centers is much larger than their width, we have $\Omega(x_1,x_2)\simeq\Omega(x_1)+\Omega(x_2)$. In the region $x_1<x_2$, $\Omega$ has a maximum in $(-x_m,x_m)$ and two saddle points in $(0,x_m)$ and $(-x_m,0)$. We assume that $x_m\gg\hbar/\sqrt{m\mu}$. The stationary solution corresponding to the maximum of $\Omega$ is shown in column 5 of Fig. 1. Those corresponding to the two saddle points [column 6 of Fig. 1 and symmetric partner $\psi(-x)$] break the symmetry of $V$ and must disappear in the linear limit.

Other extrema of $\Omega$ can be found when the centers of the two dark solitons are into the same well. In fact, when both $x_1$ and $x_2$ tend to $x_m$, or $-x_m$, the value of $\Omega(x_1,x_2)\sim$const.$-V(x_1)-V(x_2)$ increases until $|x_1-x_2|\gg\hbar/\sqrt{m\mu}$. When the distance $|x_1-x_2|$ becomes comparable with the soliton width, the two density holes in $|\psi_{\mu 2}|^2$ begin to merge and the norm of $\psi_{\mu 2}$ increases. This implies that $\Omega$ decreases for $|x_1-x_2|\to 0$ since, at least for $\mu$ sufficiently large, $\Omega\sim-\mu\|\psi_{\mu 2}\|^2$. As a consequence, $\Omega$ has two maxima in $(x_m-\delta,x_m+\delta)$ and $(-x_m-\delta,-x_m+\delta)$ with $2\delta\gtrsim\hbar/\sqrt{m\mu}$. The corresponding solutions [column 7 of Fig. 1 and symmetric

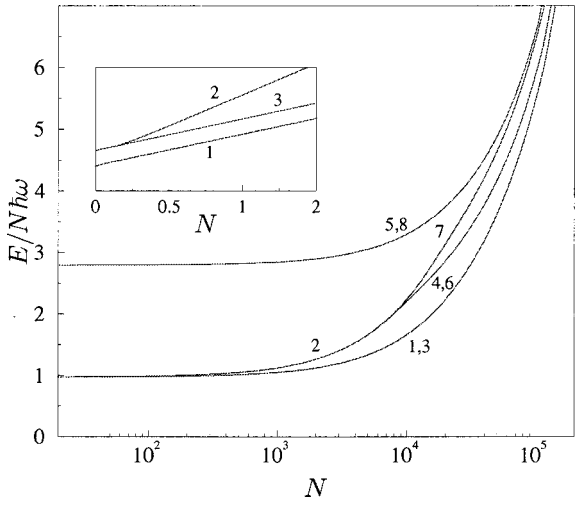


FIG. 3. Single-particle energies $E/N$ for the states shown in Fig. 1 as a function of $N$. The numbers correspond to the columns of Fig. 1. The curve 8 corresponds to the antisymmetric partner of 5.

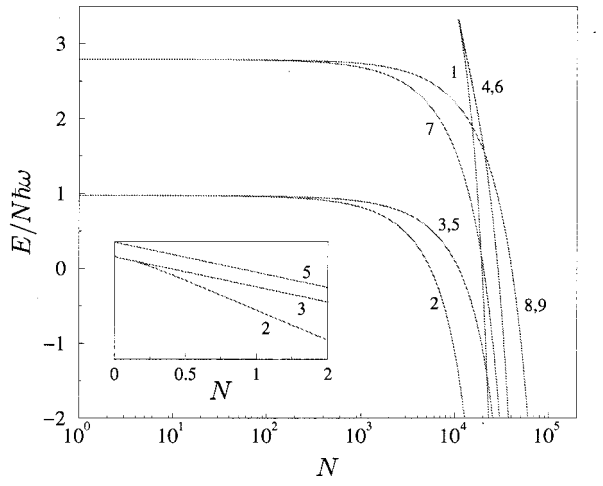


FIG. 4. As in Fig. 3 for the states shown in Fig. 2. Curves 8 and 9 correspond to the stationary solutions, not shown in Fig. 2, having as a linear counterpart the Schrödinger eigenfunctions with 2 and 3 nodes, respectively.

partner $\psi(-x)$], break the symmetry of $V(x)$ and do not have a linear counterpart.

In the attractive case the situation is more complicated. The bright solitons in the stationary solutions with linear counterpart given by Eq. (6) are multiplied by a phase factor which is alternatively $+1$ and $-1$. In general, we can expect bright solitons with arbitrary relative phases since each sech function is, for $\mu \to -\infty$, a solution of the GPE and this equation is invariant under a global phase change. Restricting to real solutions, in the two-soliton case we have to consider the following possibilities:

$$\psi^{\pm}_{\mu 1}(x) = \sqrt{\frac{2\mu}{U_0}} \left[ \operatorname{sech}\left( \frac{\sqrt{-2m\mu}}{\hbar}(x-x_0) \right) \pm \operatorname{sech}\left( \frac{\sqrt{-2m\mu}}{\hbar}(x-x_1) \right) \right]. \tag{8}$$

The functions $\Omega^{\pm}(x_0,x_1)$ obtained by inserting these expressions in Eq. (7) present, in analogy with the repulsive case, a minimum in $(-x_m,x_m)$ and two saddle points in $(0,x_m)$ and $(-x_m,0)$. The stationary states corresponding to the minimum of $\Omega^{\pm}(x_0,x_1)$ are shown in columns 3 and 5 of Fig. 2. Those corresponding to the two saddle points [columns 4 and 6 of Fig. 2 and symmetric partners $\psi^{\pm}(-x)$] break the symmetry of $V$ and do not have a linear counterpart.

On the other hand, due to the gradient term in Eq. (7), we have a different behavior of $\Omega^+$ and $\Omega^-$ when both the soliton centers $x_0$ and $x_1$ move toward the minimum of the same well. In fact, $\Omega^+$ does not present extrema while $\Omega^-$ has two minima in $(x_m-\delta,x_m+\delta)$ and $(-x_m-\delta,-x_m+\delta)$ with $2\delta \gtrsim \hbar/\sqrt{-2m\mu}$. The corresponding solutions [column 7 of Fig. 2 and symmetric partner $\psi^-(-x)$], break the symmetry of $V(x)$ and do not have a linear counterpart.

## IV. NUMERICAL SOLUTIONS WITH AN ARBITRARY NUMBER OF PARTICLES

Now we compare the zero-, one-, and two-soliton solutions discussed above with the results of numerical simulations. We use a numerical algorithm based on a standard relaxation method for partial differential equations [17]. The success of this method is crucially based on the quality of the trial functions used to start the relaxation. For $|\mu|$ very large, good trial functions are represented by the multisoliton functions with the soliton centers determined as above. The relaxed solutions can be then used as trial functions for a simulation with a smaller value of $|\mu|$. By changing $\mu$ sufficiently slowly, one can follow the evolution of the stationary states until they reach the linear limit, if it exists, or the point where they disappear. Figures 1 and 2 show in the repulsive and attractive cases, respectively, the states obtained in this way for different values of their norm $N$. For any node index $n$, the linear limit is reached when $N = N_n(\mu) \to 0$. All the solutions that break the symmetry of the external potential disappear for $N$ smaller than a critical value. However, there also exist solutions without a linear counterpart that preserve this symmetry. An example is shown in the first column of Fig. 2 which corresponds to a bright soliton at the center of the barrier.

In Figs. 3 and 4 we show the single-particle energies for the same states of Figs. 1 and 2 as a function of $N$. From these figures it is evident the generation of solutions without a linear counterpart as $N$ is increased. In the case of the attractive GPE, the stationary solution which for $N$ large is fully localized into one of the two wells (second column of Fig. 2) is, when it exists, the state of minimal energy. Therefore, the nature of the mean-field ground-state changes as a function of $N$ and this suggests the existence of a quantum phase transition in the corresponding exact many-body system.

The generation of stationary states without a linear counterpart can be understood in terms of bifurcations of superpositions of Schrödinger eigenstates. In the following we discuss an analytical example valid when the zero point energy of each isolated well, $\frac{1}{2}\hbar 2\omega$, is much smaller than the barrier height, $\omega^4/4\gamma^4$, i.e., for $\omega^3/\hbar\gamma^4 \gg 1$. Let us consider stationary solutions of the GPE of the form

$$\psi(x) = \sqrt{N}[a_0\chi_0(x-x_m) + b_0\chi_0(x+x_m)], \tag{9}$$

where $\chi_n(x)$ are the eigenfunctions of the Schrödinger problem with harmonic potential $\frac{1}{2}m(2\omega)^2x^2$ and $a_0^2+b_0^2=1$. Since the state (9) is normalized to $N$, for it to be a stationary solution of the GPE we have to extremize the energy functional $E[\psi]=\Omega[\psi]+\mu N$. Up to exponentially small terms we get

$$E(b_0) \sim b_0\sqrt{1-b_0^2} + \operatorname{sgn}(U_0)\frac{N}{N_0}(1+2b_0^4-2b_0^2), \tag{10}$$

where

$$N_0 \sim \frac{\omega^3}{\hbar\gamma^4}\exp\left(-\frac{\omega^3}{\hbar\gamma^4}\right)\sqrt{\hbar^3\omega/mU_0^2}. \tag{11}$$

For $N \ll N_0$, $E(b_0)$ has a minimum for $b_0 = 2^{-1/2}$ and a maximum for $b_0 = -2^{-1/2}$. These extrema correspond to the lowest-energy symmetric and antisymmetric linear states (columns 1 and 3 of Fig. 1 and columns 3 and 5 of Fig. 2). If $U_0 > 0$, for $N \simeq N_0$ the maximum at $b_0 = -2^{-1/2}$ bifurcates in a minimum and a maximum which, increasing $N$, moves to $b_0 = 0$. This describes the birth of the state in the second column of Fig. 1 and its subsequent localization in the right well ($a_0 = 1$). If $U_0 < 0$ a similar result is obtained with maxima and minima exchanged (see column 2 of Fig. 2). Generation of other states can be obtained by considering superpositions more complicated than Eq. (9).

## V. STABILITY OF STATIONARY SOLUTIONS

In this section we discuss the stability of the stationary states described above. We start with a linear stability analysis. Consider the linearization of Eq. (1) for a small change $\delta\Psi$ of its solution

$$i\hbar\frac{\partial}{\partial t}\delta\Psi=\left[-\frac{\hbar^2}{2m}\nabla^2+V(\boldsymbol{x})+2U_0|\Psi|^2\right]\times\delta\Psi+U_0\Psi^2\delta\Psi^*. \tag{12}$$

We are interested to evaluate the evolution of the variation $\delta\Psi$ of a stationary solution $\Psi_{\mu n}$. By writing

$$\Psi+\delta\Psi=\Psi_{\mu n}(\boldsymbol{x},t)+\delta\Psi(\boldsymbol{x},t)=e^{-i/\hbar\mu t}[\psi_{\mu n}(\boldsymbol{x})+\delta\phi(\boldsymbol{x},t)], \tag{13}$$

according to Eq. (12) the variation $\delta\phi$ and its complex conjugated $\delta\phi^*$ are determined by

$$i\hbar\frac{\partial}{\partial t}\begin{pmatrix}\delta\phi\\ \delta\phi^*\end{pmatrix}=\begin{pmatrix}\mathcal{D}_{\mu n} & U_0\psi_{\mu n}^2\\ -U_0\psi_{\mu n}^{*\,2} & -\mathcal{D}_{\mu n}\end{pmatrix}\begin{pmatrix}\delta\phi\\ \delta\phi^*\end{pmatrix}, \tag{14}$$

where

$$\mathcal{D}_{\mu n}=-\frac{\hbar^2}{2m}\nabla^2+V(\boldsymbol{x})+2U_0|\psi_{\mu n}|^2-\mu. \tag{15}$$

The solution of Eq. (14) can be written as

$$\begin{pmatrix}\delta\phi(\boldsymbol{x},t)\\ \delta\phi(\boldsymbol{x},t)^*\end{pmatrix}=\sum_k c_k e^{-i\lambda_k t/\hbar}\begin{pmatrix}f_k(\boldsymbol{x})\\ g_k(\boldsymbol{x})\end{pmatrix}, \tag{16}$$

where $\lambda_k$ and $(f_k,g_k)$ are the eigenvalues and the eigenvectors of the linearization operator

$$\begin{pmatrix}\mathcal{D}_{\mu n} & U_0\psi_{\mu n}^2\\ -U_0\psi_{\mu n}^{*\,2} & -\mathcal{D}_{\mu n}\end{pmatrix}\begin{pmatrix}f_k\\ g_k\end{pmatrix}=\lambda_k\begin{pmatrix}f_k\\ g_k\end{pmatrix} \tag{17}$$

and the coefficients $c_k$ are fixed by the initial condition $\delta\phi(\boldsymbol{x},0)$. Multiplying Eq. (17) by $(f_k^*,-g_k^*)$ and integrating over space, we get

$$\int[f_k^*\mathcal{D}_{\mu n}f_k+g_k^*\mathcal{D}_{\mu n}g_k+U_0(f_k^*g_k+f_kg_k^*)]\mathrm{d}\boldsymbol{x}=\lambda_k\int(|f_k|^2-|g_k|^2)\mathrm{d}\boldsymbol{x}. \tag{18}$$

If $\|f_k\|\neq\|g_k\|$ for any $k$, Eq. (18) implies that all the linearization eigenvalues are real so that Eq. (14) admits only quasiperiodic solutions. If $\|f_{\bar{k}}\|=\|g_{\bar{k}}\|$ for some $\bar{k}$, the corresponding linearization eigenvalue $\lambda_{\bar{k}}$ may be complex. In this case, the corresponding stationary state $\psi_{\mu n}$ can show exponential instability whenever the initial variation $\delta\phi(\boldsymbol{x},0)$ has a superposition coefficient $c_{\bar{k}}\neq0$ [18]. To check the existence of complex linearization eigenvalues, we have solved numerically the eigenvalue problem (17) by representing the linearization operator with a finite difference scheme. We find that the stationary states $\psi_{\mu n}$ shown in Fig. 1 have only real $\lambda_k$. This suggests linear stability of all stationary solutions with $U_0>0$. On the other hand, exponential instability is possible in the case of $U_0<0$. For instance, we find a couple of complex conjugated linearization eigenvalues for the symmetry-breaking two-soliton solution shown in the fourth column of Fig. 2.

Lyapunov stability of all the states $\Psi$ in the neighborhood of a stationary solution $\Psi_{\mu n}$ is a mathematically stronger concept of stability and certainly more relevant from an experimental point of view. This kind of stability was previously studied in the case of a lattice model which reduces to the GPE in the continuum limit [19]. In that paper it was shown numerically that the maximum Lyapunov exponent associated to a discretized version of Eq. (12) vanishes when the initial state $\Psi(\boldsymbol{x},0)$ is sufficiently close to one of the stationary states. A similar analysis can be pursued in the case of the GPE by simulating a huge finite-dimensional system, namely, that obtained by applying a finite difference scheme to the partial differential equation (1). Of course, the large but finite number of degrees of freedom used in the simulation sets a limit to the maximum time at which the properties of the infinite-dimensional system corresponding to the GPE are correctly represented. We will report on this elsewhere. Here we note that the gained scenario is consistent with Kuksin theory [20] which asserts that Eq. (12) admits $N$-dimensional invariant tori, deformation of Eq. (16), in a finite neighborhood of any stationary state whose linearization spectrum satisfy nondegeneracy and nonresonance conditions.

The spectrum of the linearization operator is useful also for discussing the stability of the stationary states under the effect of a dissipative perturbation. The grand-potential (7) evaluated for a state of the form (13), up to the second order in the variation $\delta\phi$ gives

$$\Omega[\Psi+\delta\Psi]=\Omega[\psi_{\mu n}]+\delta^2\Omega, \tag{19}$$

where

$$\delta^2\Omega=\frac{1}{2}\int\delta\phi^*[\mathcal{D}_{\mu n}\delta\phi+U_0\psi_{\mu n}^2\delta\phi^*]\mathrm{d}\boldsymbol{x}+\frac{1}{2}\int\delta\phi[\mathcal{D}_{\mu n}\delta\phi^*+U_0\psi_{\mu n}^{*\,2}\delta\phi]\mathrm{d}\boldsymbol{x}. \tag{20}$$

By using Eqs. (14) and (16) and the sum rule

$$\sum_k c_k e^{-i\lambda_k t/\hbar}f_k=\sum_k c_k^* e^{i\lambda_k t/\hbar}g_k^*, \tag{21}$$

we get

$$\delta^2\Omega=\frac{1}{2}\sum_k|c_k|^2\lambda_k(\|f_k\|^2-\|g_k\|^2). \tag{22}$$

Therefore, a stationary solution $\psi_{\mu n}$ is a local minimum of the grand-potential functional if and only if for any $k$ we have [21]

$$\lambda_k(\|f_k\|^2-\|g_k\|^2)\geqslant0. \tag{23}$$

To verify the disequalities (23), we resort again to the numerical solution of the eigenvalue problem (17). In the

repulsive case $U_0>0$, the condition (23) is fulfilled only by the state in the first column of Fig. 1. In the attractive case $U_0<0$, no one of the states shown in Fig. 2 satisfies Eq. (23). This can be explained observing that the grand potential evaluated at a stationary state is

$$\Omega[\psi_{\mu n}]=-\frac{1}{2}\,U_0\int|\psi_{\mu n}|^4 d\mathbf{x}. \tag{24}$$

Thus, if $U_0<0$, $\Omega$ assumes the minimal value for the trivial solution $\psi=0$. These results have a certain interest on the stability of a physical condensate in which a dissipative dynamic is introduced by the coupling with the environment degrees of freedom. Eventually the system will converge to a local minimum of $\Omega$. For attractive interaction, this implies the disappearance of the condensate. An estimate of the characteristic lifetimes has been given in the case of a vortex state [22].

We conclude our stability analysis by considering the short-time behavior of the stationary states under the action of an initial finite deformation. A similar analysis has been considered in [23] to check the stability of the solutions found in [10]. The authors of [23] studied the evolution of stationary states initially perturbed with a stochastic noise. In our case, the stationary solutions corresponding to solitons located near the extrema of the double-well potential should have great sensitivity, especially in the case of unstable extrema, to symmetry-breaking perturbations. Here, we consider the evolution of shifted stationary states, i.e., we solve Eq. (1) with the initial condition $\Psi(x,0)=\psi_{\mu n}(x-\Delta x)$. The numerical simulations have been performed with the improved Crank-Nicholson scheme introduced in [19] which provides an accurate conservation of the constants of motion of Eq. (1), namely, norm and energy. As an example, we describe the evolution of the states of column 4 of Figs. 1 and 2. Note that these are states without linear counterpart.

The state with one dark soliton has a rather simple evolution. The qualitative shape of the state does not change but the soliton oscillates around the minimum $x=x_m$ of the right well. The position of the soliton center, $x_1$, as a function of time is shown in the upper panel of Fig. 5 for $\Delta x=0.3$ $\mu$m. The amplitude of the oscillations is very small in the case considered and increases by increasing $\Delta x$. For a shift $\Delta x$ sufficiently large the soliton can jump between the two wells.

The dynamics of the state with two bright solitons is more complicated, see lower panel of Fig. 5. Initially the soliton at the center of the barrier moves toward that located inside the right well, the latter being essentially at rest. When the distance between the two solitons becomes comparable to their width the oscillations of the solitons inside the same well turn out to be correlated. The solitons do not cross each other. When the potential energy of the barrier, $V|\Psi|^2$, is sufficiently reduced by the negative interaction energy, $\frac{1}{2}U_0|\Psi|^4$, the soliton which was originally at the center of the barrier can jump into the left well. This interwell dynamic is obtained also for values of the initial shift smaller

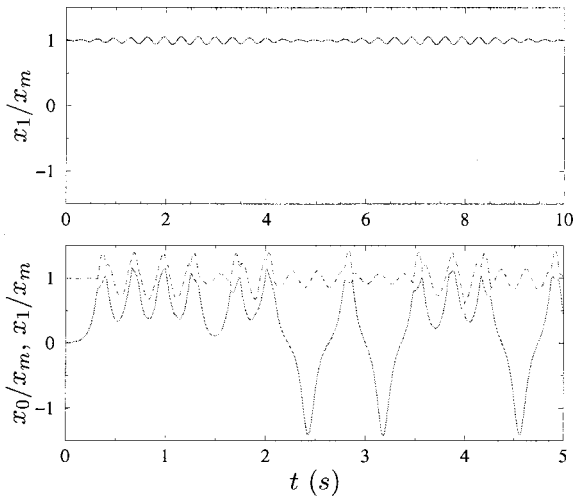


FIG. 5. Time evolution of the soliton centers for initially perturbed stationary states $\Psi(x,0)=\psi_{\mu n}(x-\Delta x)$ with $\Delta x=0.3$ $\mu$m. In the upper panel $\psi_{\mu n}$ is one of the states in column 4 of Fig. 1 while in the lower panel one of those in column 4 of Fig. 2.

than $\Delta x=0.3$ $\mu$m which is the case shown in Fig. 5. By decreasing $\Delta x$, the initial falling of the soliton at the center of the barrier into the right well (left well for $\Delta x<0$) is slowed down.

The results shown in Fig. 5 can be generalized to different kinds of perturbations, e.g., stochastic noise, modification of the parameters of the external potential. Details will be reported elsewhere.

## VI. CONCLUSIONS

We have shown that in presence of an external potential a 1D GPE can admit stationary solutions without a linear counterpart. Their existence is strictly connected to the multiwell nature of the potential. In the double-well example discussed here, these solutions disappear in the limit $\omega\to 0$ when the potential assumes the shape of a single quartic well. For a piece-wise constant double well, the stationary states here discussed analytically only in the limit of strong nonlinearity can be obtained in terms of Jacobi elliptic functions for any number of particles in the condensate.

We have also discussed the stability of the stationary states under different points of view. The results indicate that the solitonlike states, with and without a linear counterpart, are sufficiently stable for times shorter than few tenths of seconds. This is the time scale explored in the BEC experiments [11,12]. By voluntarily introducing perturbations of proper intensity, a soliton dynamics could also be observed.

## ACKNOWLEDGMENTS

We thank R. Onofrio for very useful comments on the experimental aspects of BEC and a critical reading of the manuscript. This work was supported in part by Cofinanziamento MURST protocollo MM02263577_001.

[1] L.P. Pitaevskii, in *Bose-Einstein Condensation in Atomic Gases*, Proceeding of the International School of Physics ''Enrico Fermi,'' Course 140, 1998, edited by M. Inguscio, S. Stringari, and C. Wieman (IOS Press, Amsterdam, 1999), p. 287.
[2] V.I. Yukalov, E.P. Yukalova, and V.S. Bagnato, Phys. Rev. A **56**, 4845 (1997); Laser Phys. **10**, 26 (2000).
[3] Y.S. Kivshar, T.J. Alexander, and S.K. Turitsyn, Phys. Lett. A **278**, 225 (2001).
[4] M.R. Matthews *et al.*, Phys. Rev. Lett. **83**, 2498 (1999).
[5] K.W. Madison *et al.*, Phys. Rev. Lett. **84**, 806 (2000).
[6] C. Raman *et al.*, Phys. Rev. Lett. **83**, 2502 (1999); R. Onofrio *et al.*, *ibid.* **85**, 2228 (2000).
[7] S. Burger *et al.*, Phys. Rev. Lett. **83**, 5198 (1999).
[8] J. Denschlag *et al.*, Science **287**, 97 (2000).
[9] R. D'Agosta, B.A. Malomed, and C. Presilla, Phys. Lett. A **275**, 424 (2000).
[10] L.D. Carr, C.W. Clark, and W.P. Reinhardt, Phys. Rev. A **62**, 063610 (2000); **62**, 063611 (2000).
[11] M.R. Andrews, C.G. Townsend, H.-J. Miesner, D.S. Durfee, D.M. Kurn, and W. Ketterle, Science **275**, 637 (1997).
[12] F.S. Cataliotti, S. Burger, C. Fort, P. Maddaloni, F. Minardi, A. Trombettoni, A. Smerzi, and M. Inguscio, Science **293**, 843 (2001).
[13] J.C. Eilbeck, P.S. Lomdahl, and A.C. Scott, Physica D **16**, 318 (1985).
[14] A. Smerzi, S. Fantoni, S. Giovanazzi, and S.R. Shenoy, Phys. Rev. Lett. **79**, 4950 (1997).
[15] G.J. Milburn, J. Corney, E.M. Wright, and D.F. Walls, Phys. Rev. A **55**, 4318 (1997).
[16] E.A. Ostrovskaya, Y.S. Kivshar, M. Lisak, B. Hall, F. Cattani, and D. Anderson, Phys. Rev. A **61**, 031601(R) (2000).
[17] H. Press, B.P. Flannery, S.A. Teukolsky, and W.T. Vetterling, *Numerical Recipes* (Cambridge University Press, Cambridge, 1989), Chap. 16.
[18] D.V. Skryabin, Phys. Rev. A **63**, 013602 (2000).
[19] P. Castiglione, G. Jona-Lasinio, and C. Presilla, J. Phys. A **29**, 6169 (1996).
[20] S.B. Kuksin, *Nearly Integrable Infinite Dimenional Hamiltonian Systems*, Lecture Notes in Mathematics Vol. 1556 (Springer-Verlag, Berlin, 1993).
[21] J.J. Garcia-Ripoll and V.M. Perez-Garcia, Phys. Rev. A **60**, 4864 (1999).
[22] P.O. Fedichev and G.V. Shlyapnikov, Phys. Rev. A **60**, R1779 (1999).
[23] L.D. Carr, J.N. Kutz, and W.P. Reinhardt, Phys. Rev. E **63**, 066604 (2001).